Simultaneous DNP Enhancements of ^{1}H and ^{13}C nuclei: theory and experiments

Daphna Shimon, Yonatan Hovav, Ilia Kaminker, Akiva Feintuch, Daniella Goldfarb

and Shimon Vega*

Department of Chemical Physics, Weizmann Institute of Science, Rehovot, Israel
*E-mail: Shimon.Vega@weizmann.ac.il

1 DNP on model a system containing two electrons and a ^{13}C and a ^{1}H nucleus

In the four spin system, $\{e_a - e_b - (^1\mathrm{H},^{13}\mathrm{C})\}$, described in the main text, we recognize 8 different degeneracies that are possible by changing the difference between the frequencies of the electrons. These degeneracies are shown in Fig. 3 and listed in Table 1 in the main text. Conditions (2,2') and (4,4') are the standard CE-DNP conditions for ^{1}H and ^{13}C , $|\omega_a - \omega_b| = \omega_n$ with $n = {}^1$H or ^{13}C, and the conditions (1,1') and (3,3') are the higher order CE-DNP conditions $|\omega_a - \omega_b| = \omega_H + \omega_C$ and $|\omega_a - \omega_b| = \omega_H - \omega_C$, respectively. The following figures show different aspects of this four spin system at the different CE conditions, including energy level diagrams and simulated DNP spectra.

Fig. S1 shows the energy level diagram at ^{13}C-CE condition (4), with some of the different transitions highlighted such as the overlapping CE transitions in blue and the "proton shifted ^{13}C-CE" transitions in red.

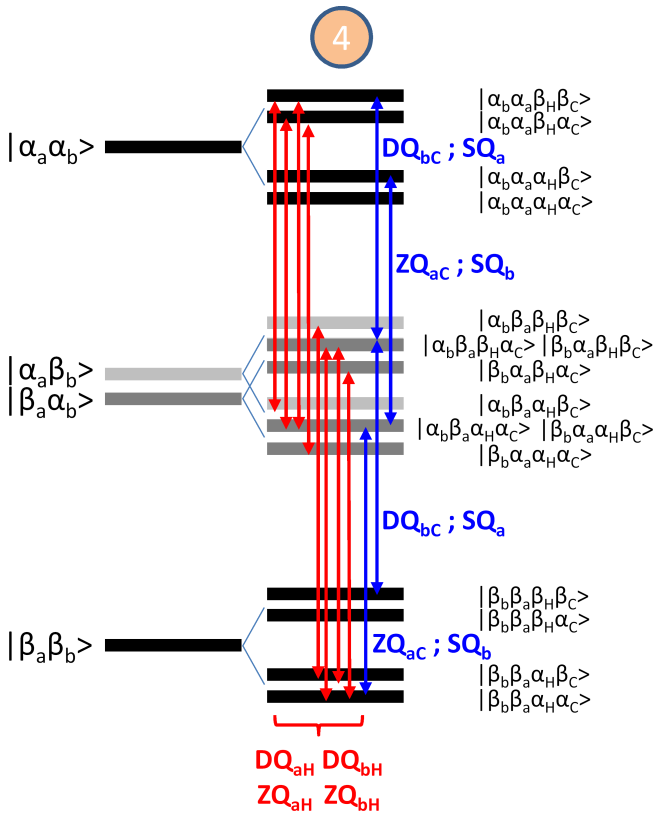

Fig. S1: Energy level diagrams of a four spin system, $\{e_a - e_b - (^1\mathrm{H}, ^{13}\mathrm{C})\}$, at the ^{13}C-CE condition (4). The transitions plotted in blue are the CE transitions, and in red are the other overlapping transitions: ZQ_{aH} with ZQ_{bC}, DQ_{bH} with DQ_{aC}, DQ_{bH} with DQ_{aC}, and ZQ_{aH} with ZQ_{bC}.

The enhancements of "proton shifted ^{13}C-CE" (transitions marked in red in the main text in Fig. 4) are highly dependent on the relaxation times in the system. Inspecting the intensity of the enhancements induced by the proton shifted ^{13}C-CE as a function of different relaxation times we observed that the value of T_{1C} does not affect these intensities, while T_{1H} and T_{1e} have a strong effect. These effects are shown in Fig. S2. There the ^{13}C polarization as a function of different relaxation times is plotted by zooming in on the low frequency dipolar line of the positive enhancement peak of the proton shifted ^{13}C-CE: $\omega_{MW} = \mathrm{DQ}_{bH}$. The black peak is the exact data shown in the main text in Fig. 4. If we lengthen the T_{1H} we see a large decrease in ^{13}C polarization (red), if we shorten T_{1C} we only detect a small decrease (magenta), and if we shorten T_{1e} we again see a large decrease of the ^{13}C polarization (blue). The actual values of the different parameters are given in the legend and figure caption.

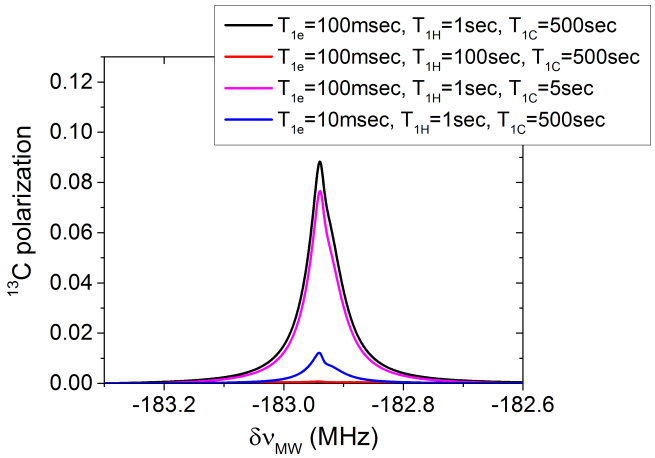

Fig. S2: Simulated DNP spectra of the four spin system $\{e_a - e_b - (^1\mathrm{H}, ^{13}\mathrm{C})\}$ at the ^{13}C-CE condition (condition 4). Plotted in the y-axis is the ^{13}C polarization with respect to the electron polarizations at thermal equilibrium. The x axis is zoomed in on the low frequency dipolar line of the positive enhancement peak of the proton shifted ^{13}C-CE: $\delta\nu_{MW} = \mathrm{DQ}_{bH}$. The MW frequency scale is given with respect to $\nu_{ref} = 95 \cdot 10^3$ MHz: $\delta\nu_{MW} = \omega_{MW}/2\pi - \nu_{ref}$. The ^{13}C polarization is plotted as a function of the different relaxation times: (black) $T_{1e} = 100$ msec, $T_{1H} = 1$ sec, $T_{1C} = 500$ sec, (red) $T_{1e} = 100$ msec, $T_{1H} = 100$ sec, $T_{1C} = 500$ sec, (magenta) $T_{1e} = 100$ msec, $T_{1H} = 1$ sec, $T_{1C} = 5$ sec, (blue) $T_{1e} = 10$ msec, $T_{1H} = 1$ sec, $T_{1C} = 500$ sec. The baseline polarization which results from off-resonance CE enhancement was removed in all four cases, in order to simplify the comparison of intensities. The other parameters used to simulate the DNP spectra are: $T = 10$ K, $\omega_a = 95$ GHz, $\omega_b = 94.9641$ GHz, $\omega_H = 144$ MHz, $\omega_C = 36$ MHz, $D_{ab} = 3$ MHz, $A_{z,aH} = A_{z,bH} = 0$ MHz, $A_{z,aC} = A_{z,bC} = 0$ MHz, $A^{\pm}_{aH} = 0.5$ MHz, $A^{\pm}_{bH} = 0$ MHz, $A^{\pm}_{aC} = 0.125$ MHz, $A^{\pm}_{bC} = 0$ MHz, $d_{HC} = 0$ MHz, $\omega_1 = 0.5$ MHz, $T_{2e} = 20$ usec, $T_{2n} = 100$ usec.

Next we show the simulated DNP spectra for the four spin system, $\{e_a - e_b - (^1\mathrm{H},^{13}\mathrm{C})\}$, at the standard ^{1}H-CE condition (see Fig. S3). In this case the parameters chosen for the simulation do not result the "carbon shifted ^{1}H-CE" peaks (they should have appeared at the frequencies of the red arrows) in the ^{1}H spectrum, but there is some "double SE" visible in the ^{13}C spectrum at the high frequency side.

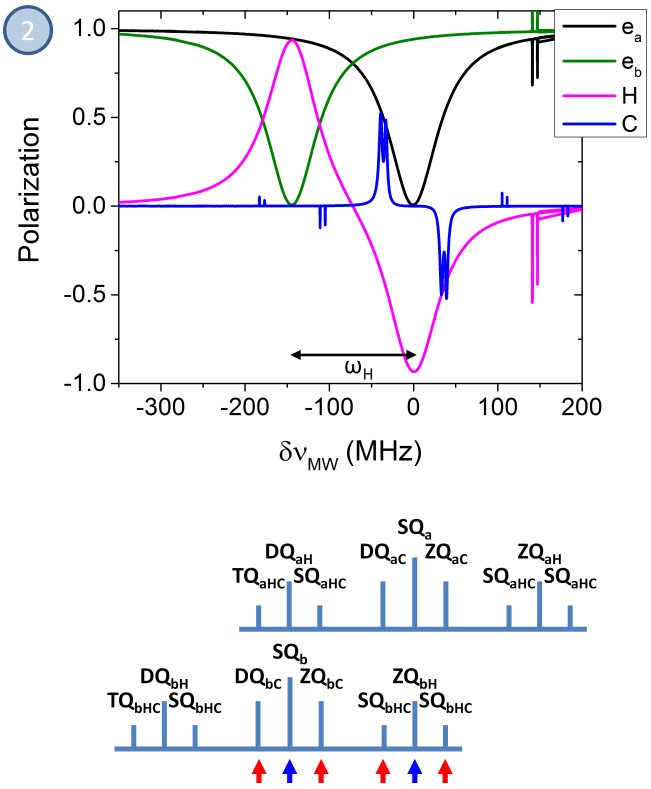

Fig. S3: Simulated DNP spectra of the four spin system $\{e_a - e_b - (^1\mathrm{H},^{13}\mathrm{C})\}$ at the ^{1}H-CE condition (2). Plotted are the normalized ^{1}H (magenta), ^{13}C (blue) and electron (black, green) polarizations with respect to the electron polarizations at thermal equilibrium. The MW frequency scale is given with respect to $\nu_{ref} = 95 \cdot 10^3$ MHz: $\delta\nu_{MW} = \omega_{MW}/2\pi - \nu_{ref}$. At the bottom are plotted the transitions of the system. The blue arrows mark the overlapping ^{1}H-CE transitions. The red arrows mark the "carbon shifted ^{1}H-CE" transitions: DQ_{aC}, ZQ_{aC}, DQ_{bC} and ZQ_{bC}, but they are not visible in the ^{1}H spectrum with the parameters chosen. The parameters used to simulate the DNP spectra are: $T = 10$ K, $\omega_a = 95$ GHz, $\omega_b = 94.8560$ GHz, $\omega_H = 144$ MHz, $\omega_C = 36$ MHz, $D_{ab} = 3$ MHz, $A_{z,aH} = A_{z,bH} = 0$ MHz, $A_{z,aC} = A_{z,bC} = 0$ MHz, $A^{\pm}_{aH} = 0.5$ MHz, $A^{\pm}_{bH} = 0$ MHz, $A^{\pm}_{aC} = 0.125$ MHz, $A^{\pm}_{bC} = 0$ MHz, $d_{HC} = 0$ MHz, $\omega_1 = 0.5$ MHz, $T_{1e} = 100$ msec, $T_{1H} = 100$ sec, $T_{1C} = 500$ sec, $T_{2e} = 20$ usec, $T_{2n} = 100$ usec.

In Fig. S4 we plot the energy level diagram of the four spin system, $\{e_a - e_b - (^1\mathrm{H}, ^{13}\mathrm{C})\}$, at the two spin ^{1}H-^{13}C-CE condition (3). Highlighted in blue are the transitions that are overlap due to the CE condition, and in red are other overlapping transitions.

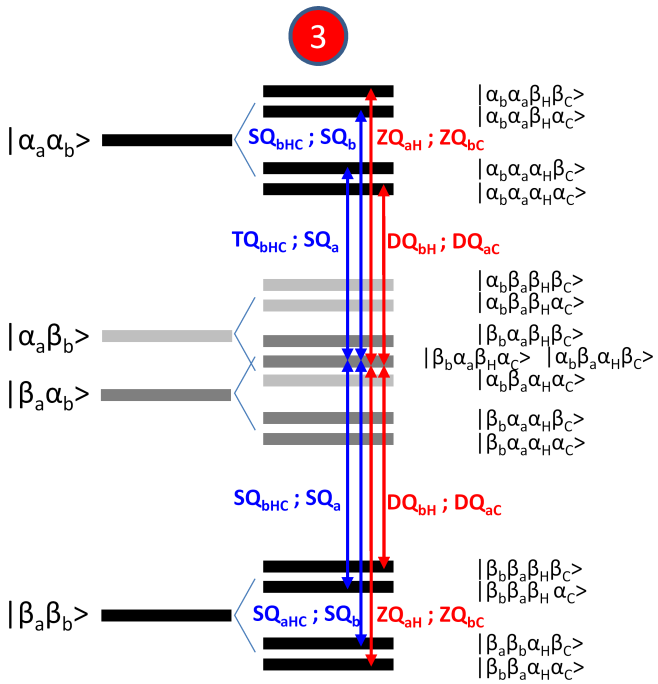

Fig. S4: Energy level diagrams of a four spin system, $\{e_a - e_b - (^1\mathrm{H}, ^{13}\mathrm{C})\}$, at the ^{1}H-^{13}C-CE condition (3). The transitions plotted in blue are the CE transitions, and in red are the transitions of the "proton shifted ^{13}C-CE": DQ_{aH}, DQ_{bH}, ZQ_{aH} and ZQ_{bH}.

Next we show the simulated DNP spectra for the four spin system, $\{e_a - e_b - (^1\mathrm{H},^{13}\mathrm{C})\}$, at the heteronuclear ^{1}H-^{13}C-CE condition (1) (see Fig. S5). The large CE enhancements of both the ^{1}H (magenta) and the ^{13}C (blue) are clearly observed. The ^{1}H polarization is lower than the ^{13}C polarization due to its shorter T_{1H} value. A description of the ^{13}C and ^{1}H polarizations at the heteronuclear CE conditions (1,1'; 3,3') will be shown in Fig. 6.

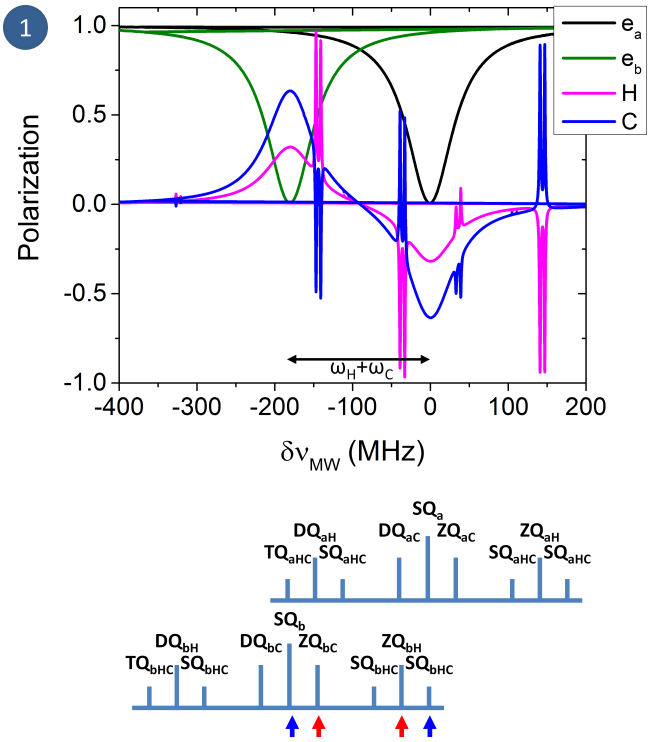

Fig. S5: Simulated DNP spectra of the four spin system $\{e_a - e_b - (^1\mathrm{H},^{13}\mathrm{C})\}$ at the ^{1}H-^{13}C-CE condition (1). Plotted are the ^{1}H (magenta), ^{13}C (blue) and electron (black, green) polarizations with respect to the electron polarizations at thermal equilibrium. The MW frequency scale is given with respect to $\nu_{ref} = 95 \cdot 10^3$ MHz: $\delta\nu_{excite} = \omega_{excite}/2\pi - \nu_{ref}$. At the bottom are plotted the transitions of the system. The blue arrows mark the overlapping high order CE transitions. The red arrows mark the overlapping transitions: DQ_{aH} with ZQ_{bC} and ZQ_{bH} with DQ_{aC}. The parameters used to simulate the DNP spectra are: $T = 10$ K, $\omega_a = 95$ GHz, $\omega_b = 94.820$ GHz, $\omega_H = 144$ MHz, $\omega_C = 36$ MHz, $D_{ab} = 3$ MHz, $A_{z,aH} = A_{z,bH} = 0$ MHz, $A_{z,aC} = A_{z,bC} = 0$ MHz, $A^{\pm}_{aH} = 0.5$ MHz, $A^{\pm}_{bH} = 0$ MHz, $A^{\pm}_{aC} = 0.125$ MHz, $A^{\pm}_{bC} = 0$ MHz, $\omega_1 = 0.5$ MHz, $T_{1e} = 100$ msec, $T_{1H} = 100$ sec, $T_{1C} = 200$ sec, $T_{2e} = 20$ usec, $T_{2n} = 100$ usec.

1.1 The $\{^1\mathrm{H} -^{13}\mathrm{C}\}$ heteronuclear CE mechanism {1,1' ; 3,3'}

In the main text we described the nuclear polarizations in the four spin system,$\{e_a - e_b - (^1\mathrm{H},^{13}\mathrm{C})\}$, at the heteronuclear CE conditions (1 and 3), in terms of the electron polarizations and as a function of T_{1H} and T_{1C}, with the following equations:

$$P_{^1H} \pm P_{^{13}C} = \frac{P_a - P_b}{1 - P_a P_b} \tag{1}$$

$$P_{^1\mathrm{H}} = \frac{P_a - P_b}{(1 - P_a P_b)(1 + \frac{T_{1C}}{T_{1H}})} \tag{2}$$

$$P_{^{13}\mathrm{C}} = \pm\frac{P_a - P_b}{(1 - P_a P_b)(1 + \frac{T_{1H}}{T_{1C}})} \tag{3}$$

for $|\omega_a - \omega_b| = |\omega_H \pm \omega_C|$, respectively, where we define $\omega_a > \omega_b$. In Fig. S6 we show that these equations hold for many different parameters by plotting the left sides of the equation on the x axis and the right side of the equations on the y axis. (a) and (c) are calculated for CE condition 1, and (b) and (d) for CE condition 3. In (a,b) Eq. 1 is plotted for many ω_{MW}, T_{1H} and T_{1C} values, while in (c,d), Eqs. 2 (black) and 3 (magenta) are plotted for many T_{1H} and T_{1C} values. The parameters used for the simulations are given in the figure caption. As can be seen all three equations hold quite well over a wide range of parameters, as long as the conditions that the MW irradiation equally affects the two SQ_e transitions of each electron equally (splitted due to the electron-electron dipolar interaction and the secular term of the hyperfine interaction) [1]. Moreover, Eqn. (1) is also correct at thermal equilibrium while Eqns. (2) and (3) are correct only during on-resonance MW irradiation on either electron e_a or electron e_b.

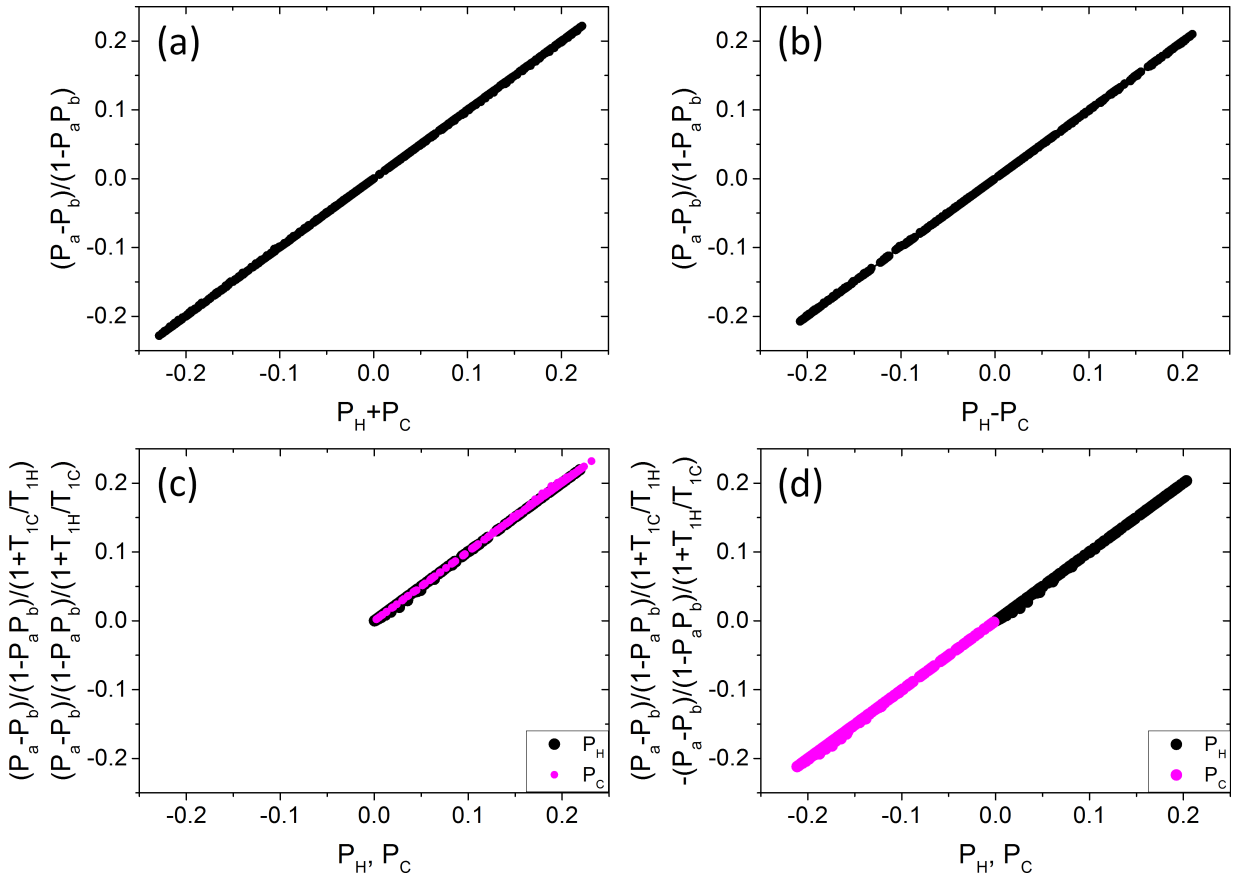

Fig. S6: (a) and (c) are calculated for CE condition 1, and (b) and (d) for CE condition 3. In (a,b) Eq. 1 is plotted for ω_{MW} between -300 MHz and 300 MHz, with $T_{1H} = 1$ sec and T_{1C} between 10 sec and 10^4 sec. In (c,d), Eqs. 2 (black) and 3 (magenta) are plotted, for T_{1H} between 1 sec and 1000 sec and T_{1C} between 10 sec and 10^4 sec, with $\omega_{MW} = \omega_b$. The other parameters of the simulation: $T = 10$ K, $\omega_a = 95$ GHz, $\omega_b = 94.820$ GHz for CE condition (1) and $\omega_b = 94.8920$ GHz for CE condition (3), $\omega_H = 144$ MHz, $\omega_C = 36$ MHz, $D_{ab} = 0.5$ MHz, $A_{z,aH} = A_{z,bH} = 0$ MHz, $A_{z,aC} = A_{z,bC} = 0$ MHz, $A^{\pm}_{aH} = 0.5$ MHz, $A^{\pm}_{bH} = 0$ MHz, $A^{\pm}_{aC} = 0.125$ MHz, $A^{\pm}_{bC} = 0$ MHz, $\omega_1 = 0.5$ MHz, $T_{1e} = 100$ msec, $T_{2e} = 20$ usec, $T_{2n} = 100$ usec.

2 Experimental results and analysis

In the following section we will discuss several aspects of the experimental DNP data and its analysis. In Fig. S7 we begin with a comparison between ^{13}C-DNP spectra measured at 10 K, (a) before and (b) after sonication of the trityl sample. This was done in order to identify the nature of the inner lineshapes the sample that appear at frequencies and do not correspond to any Larmor frequency in the system, or any combination of Larmor frequencies. Comparing the two spectra, we see that the inner pair of spectral features disappeared, while the outer pair is not affected. The disappearance of the inner pair after sonication suggests that it is related to a dimerization or clustering of the trityl radicals during sample preparation, causing large electron-electron interactions similar to what was described in Ref. [2]. It could be that after sonication these dimers or clusters are largely disrupted to a level that their DNP contributions disappear. The presence (or absence) of these dimers or clusters did not influence the EPR lineshapes, which suggests their low abundance (EPR data not shown).

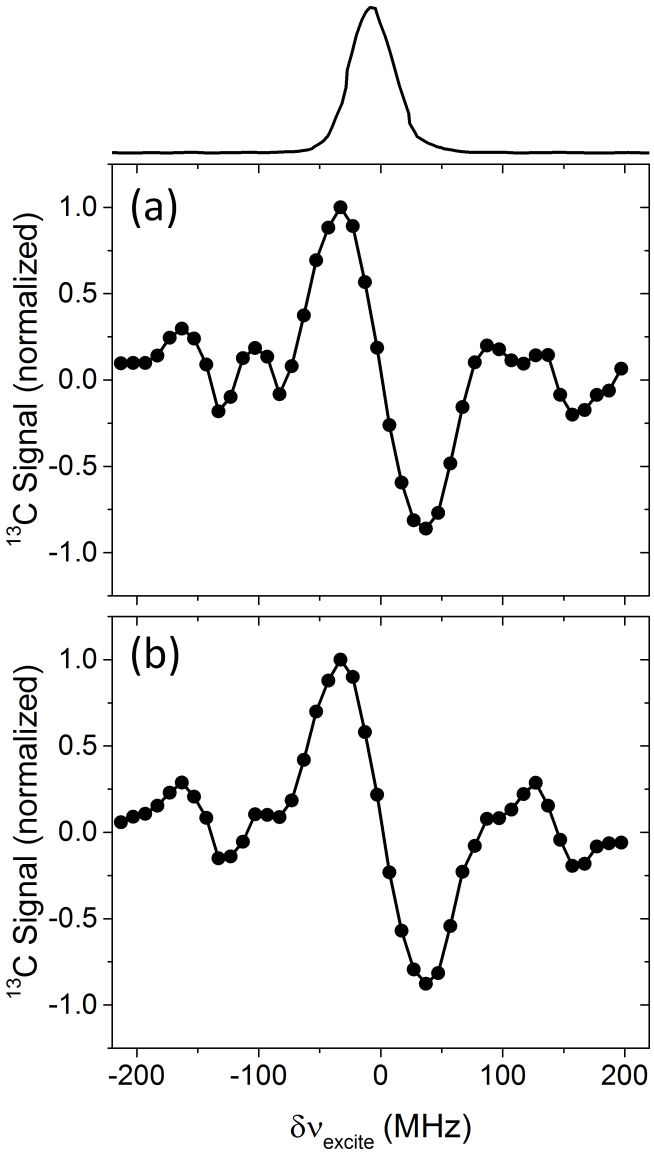

Fig. S7: Normalized ^{13}C-DNP spectra measured at 10 K with $t_{MW} = 80$ sec (a) before sonication and (b) after sonication. Plotted above is the ED-EPR spectrum of the sample before sonication. The parameters of the experiments are listed in the methods Section. The lines in this figure are to guide the eye. The MW frequency scale is given with respect to $\nu_{ref} = 94.863 \cdot 10^3$ MHz.

In Fig. S8 we plot the ELDOR spectra measured at 30 K and their analysis. The fits are not as good as at 6.5 K. This is attributed to the additional effects of electron hyperpolarization and depolarization that were previously described in Ref. [3]. The effect of this electron hyperpolarization and depolarization on the DNP spectrum is small because they appear at the edges of the EPR spectrum where the probability of finding electrons is low [3]. The parameters used for getting the ELDOR profiles, without taking these extra effects into account, are given in Table 3 in the main text.

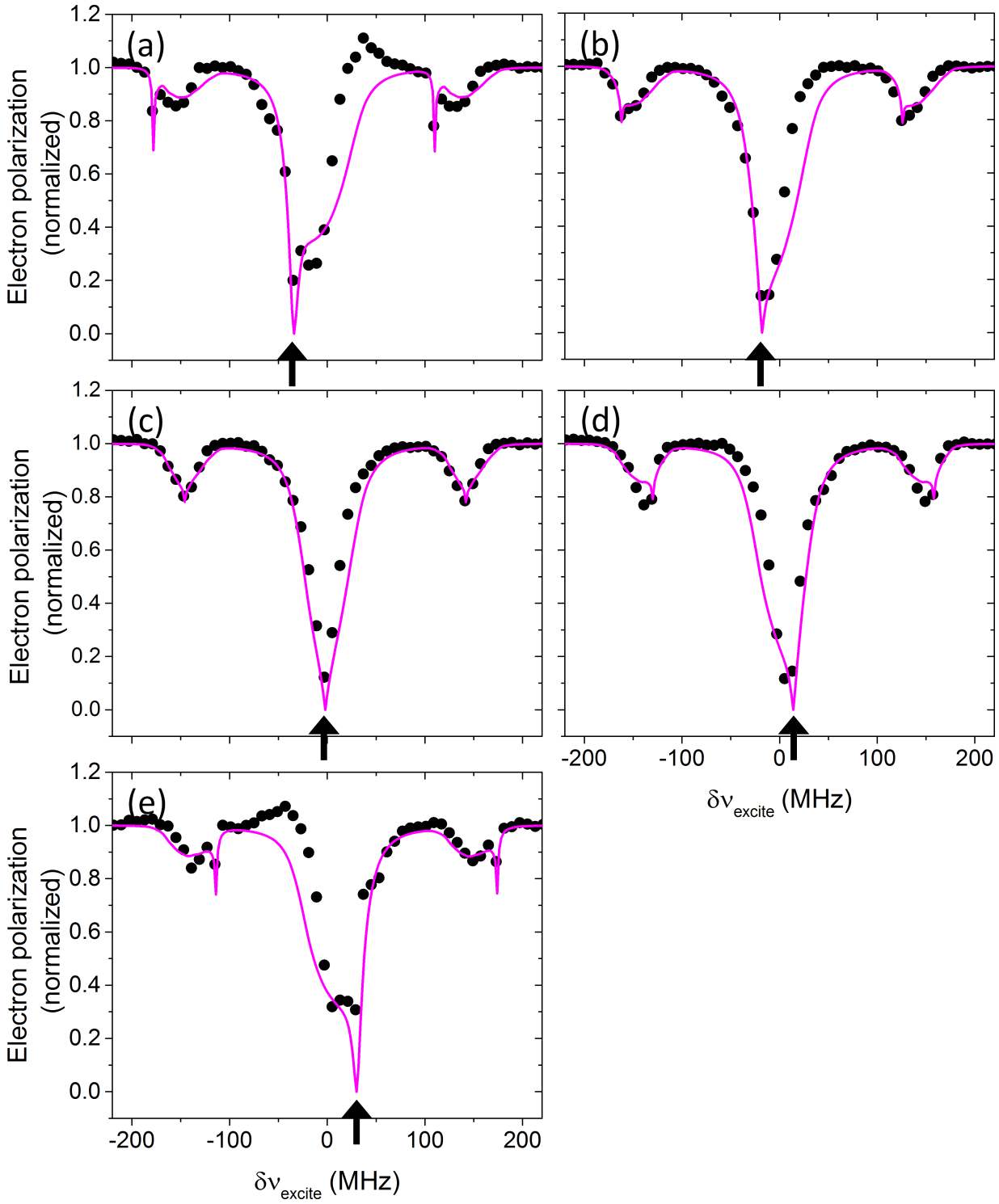

Fig. S8: Fitting of the ELDOR spectra measured at 30 K and at different ω_{detect} frequencies, marked by the black arrows. The experimental data (black circles) are overlayed on the fits (magenta lines). The black arrows mark the detection frequencies: (a) -32 MHz, (b) -16 MHz, (c) 0 MHz, (d) 16 MHz and (e) 32 MHz. The parameters used for the fitting are given in Table 3. The MW frequency scale is given with respect to $\nu_{ref} = 94.863 \cdot 10^3$ MHz.

It is also possible to plot the electron polarization, $E_e(\delta\nu_{excite}, \delta\nu_{detect})$, as 2D contour plots as a function of $\delta\nu_{excite}$ and $\delta\nu_{detect}$. Fig. S9 shows the simulated electron polarization at (a) 6.5 K and (b) 30 K. They were calculated using the parameters given in Table 3 of the main text. In the direction of the x-axis the contours clearly show the SQ_e transition around $\delta\nu_{excite} = 0$ MHz as well as the ZQ_{eH} and DQ_{eH} transitions around $\delta\nu_{excite} = \pm 144$ MHz. In the direction of the y-axis you can see the changes in the shape of the ELDOR spectra as a function of $\delta\nu_{detect}$ due to the electron spectral diffusion (eSD).

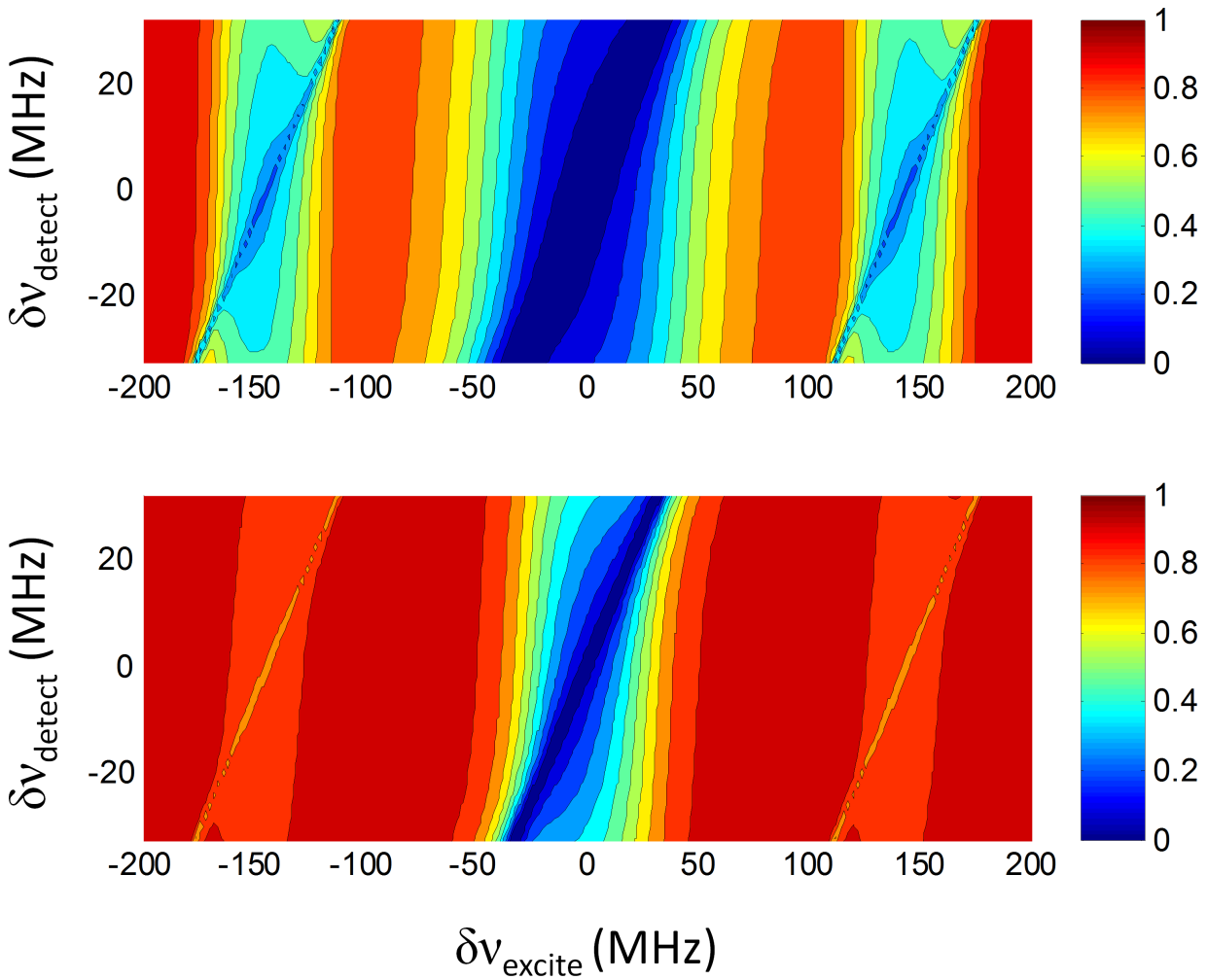

Fig. S9: Simulated 2D ELDOR contours, $Pe(\delta\nu_{detect}; \delta\nu_{excite})$, that show the electron polarization across the EPR frequency $\delta\nu_{detect}$ for different $\delta\nu_{excite}$ frequencies. The MW frequency scale is given with respect to $\nu_{ref} = 94.863 \cdot 10^3$ MHz.

Finally, in Fig. S10 we show the fits of the experimental ^{1}H-DNP spectra at (a) 6.5 K and (b) 30 K, fitted with the simulated SE-DNP spectrum, $S^H_{SE}(\delta\nu_e)$.

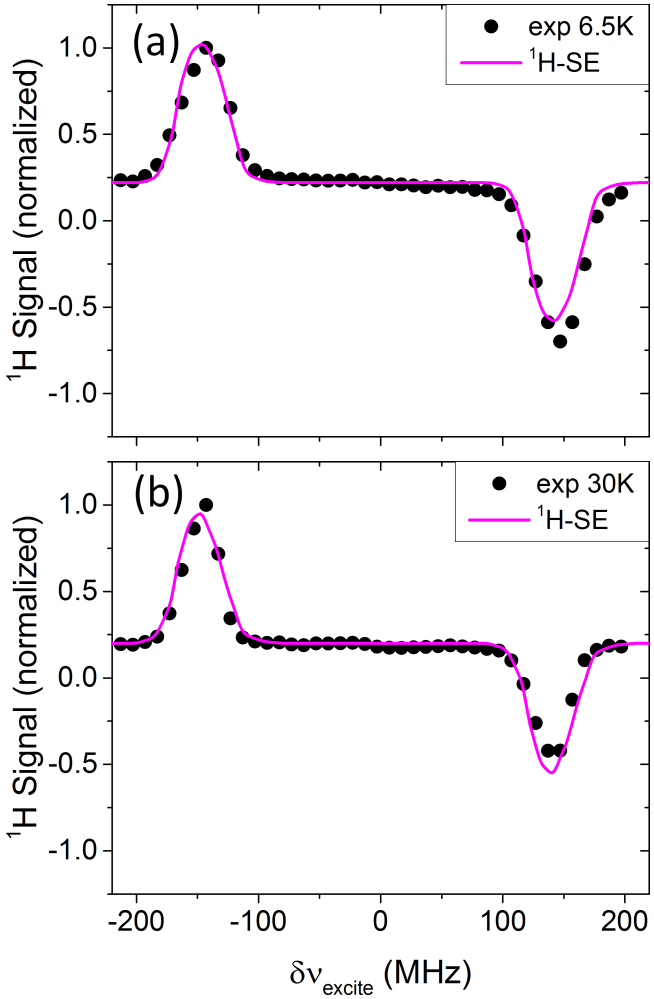

Fig. S10: ^{1}H experimental DNP spectrum measured before sonication (symbols) at (a) 6.5 K and (b) 30K overlaid with the simulated SE-DNP spectrum (magenta). The MW frequency scale is given with respect to $\nu_{ref} = 94.863 \cdot 10^3$ MHz.

References

[1] Y. Hovav, D. Shimon, I. Kaminker, A. Feintuch, D. Goldfarb and S. Vega, Phys. Chem. Chem. Phys., 2015, 17, 6053-6065.

[2] I. Marin-Montesinos, J. C. Paniagua, M. Vilaseca, A. Urtizberea, F. Luis, M. Feliz, F. Lin, S. Van Doorslaer and M. Pons, Phys. Chem. Chem. Phys., 2015, 17, 5785-5794.

[3] Y. Hovav, I. Kaminker, D. Shimon, A. Feintuch, D. Goldfarb and S. Vega, Phys. Chem. Chem. Phys., 2015, 17, 226-244.